

Lattice Matching as the Determining Factor for Molecular Tilt and Multilayer Growth Mode of the Nanographene Hexa-*peri*-hexabenzocoronene

Paul Beyer,^{†,||} Tobias Breuer,^{‡,||} Saliou Ndiaye,[‡] Anton Zykov,[†] Andreas Viertel,[§] Manuel Gensler,[†] Jürgen P. Rabe,^{†,⊥} Stefan Hecht,^{§,⊥} Gregor Witte,^{*,‡} and Stefan Kowarik^{*,†}

[†]Institut für Physik, Humboldt-Universität zu Berlin, 12489 Berlin, Germany

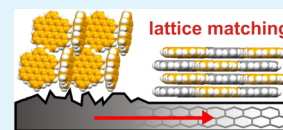
[‡]Fachbereich Physik, Philipps-Universität Marburg, 35032 Marburg, Germany

[§]Institut für Chemie, Humboldt-Universität zu Berlin, 12489 Berlin, Germany

[⊥]IRIS-Adlershof, Humboldt-Universität zu Berlin, 12489 Berlin, Germany

S Supporting Information

ABSTRACT: The microstructure, morphology, and growth dynamics of hexa-*peri*-hexabenzocoronene (HBC, C₄₂H₁₈) thin films deposited on inert substrates of similar surface energies are studied with particular emphasis on the influence of substrate symmetry and substrate–molecule lattice matching on the resulting films of this material. By combining atomic force microscopy (AFM) with X-ray diffraction (XRD), X-ray absorption spectroscopy (NEXAFS), and in situ X-ray reflectivity (XRR) measurements, it is shown that HBC forms polycrystalline films on SiO₂, where molecules are oriented in an upright fashion and adopt the known bulk structure. Remarkably, HBC films deposited on highly oriented pyrolytic graphite (HOPG) exhibit a new, substrate-induced polymorph, where all molecules adopt a recumbent orientation with planar π -stacking. Formation of this new phase, however, depends critically on the coherence of the underlying graphite lattice since HBC grown on defective HOPG reveals the same orientation and phase as on SiO₂. These results therefore demonstrate that the resulting film structure and morphology are not solely governed by the adsorption energy but also by the presence or absence of symmetry- and lattice-matching between the substrate and admolecules. Moreover, it highlights that weakly interacting substrates of high quality and coherence can be useful to induce new polymorphs with distinctly different molecular arrangements than the bulk structure.



KEYWORDS: organic semiconductor, nanographene, X-ray structure, morphology of films, polycyclic aromatic hydrocarbons

1. INTRODUCTION

Organic semiconductors consisting of π -conjugated aromatic molecules have become a focus of current research because of their promising potential for future thin-film and flexible electronic device applications.^{1,2} While optoelectronic properties of these materials are mainly determined by the spacing of molecular energy levels, charge transport in molecular solids is largely affected by the spatial overlap of orbitals of neighboring molecules.³ Owing to the anisotropic shape of aromatic molecules, these compounds generally adopt complex packing motifs in the crystalline phase, which result also in a pronounced anisotropy of electronic properties of organic crystals and crystalline molecular films.⁴ A synthetic strategy to enhance the electronic properties is based on specific chemical modifications that control the molecular electronic levels but also affect the molecular packing and intermolecular distances.^{5,6} Another approach, utilizing substrate-mediated crystallization, was demonstrated in a previous study for perfluorinated pentacene (PFP) films grown on graphene or graphite. There a new, substrate-induced polymorph with coplanar π -stacking was identified that does not exist in the bulk crystal phase of PFP and favors enhanced charge carrier mobility along the stacking direction.⁷

Of particular interest among organic semiconductors is hexa-*peri*-hexabenzocoronene (HBC, C₄₂H₁₈), a discotic, polycyclic hydrocarbon that can be considered as a hydrogen-terminated molecular version of graphene, a so-called nanographene.⁸ Its substantial thermal and radiation stability in combination with a high charge carrier mobility renders it a promising material for device applications.^{9,10} In the bulk crystal structure HBC exhibits a flattened out herringbone motif, where both molecules of the unit cell adopt an almost perpendicular arrangement as shown in Figure 1.¹¹ As an example for the aforementioned synthetic strategy, the introduction of peripheric alkyl chains results in a coplanar π -stacking packing motif and furthermore enhanced solubility, hence enabling drop casting and other solution-processing techniques.¹² Though this allows the fabrication of solution-processed field effect transistors with extended HBC monodomains,^{13–15} the obtained charge carrier mobilities are significantly lower than that of other organic semiconductor films,¹ thus lagging behind the expectations for π -stacked molecular materials. Since

Received: September 22, 2014

Accepted: November 14, 2014

Published: November 14, 2014

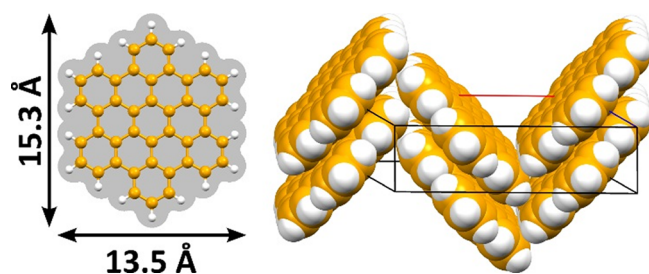


Figure 1. van der Waals dimensions and molecular bulk structure of hexa-peri-hexabenzocoronene (HBC, $C_{42}H_{18}$).¹¹

possible reasons for this noncompliance are structural defects and/or contaminations, it is desirable to pursue alternative concepts to prepare highly ordered HBC films with controlled molecular orientation—if feasible, vacuum-based to minimize contaminations. Although single-crystal substrates appear unfavorable for device applications they allow for a detailed analysis of the growth dynamics and structure of thin films, which is mandatory for a deeper understanding of controlled film preparation. The D_{6h} symmetry of HBC suggests substrate surfaces with hexagonal symmetry as natural templates. In fact, densely packed, epitaxially ordered HBC monolayer films of flat-lying molecules are formed on the (111) surface of the coinage metals Au, Ag, and Cu^{16–18} as well as on the rather inert basal planes of highly oriented pyrolytic graphite (HOPG) and MoS_2 .^{19,20} By contrast, for HBC films grown on SiO_2 or polycrystalline gold²⁰ no orientational ordering of HBC was observed because the substrate does not induce any symmetry. Remarkably, the lying molecular orientation of HBC is also maintained in thin multilayers up to 3 ML on Cu(111) and Au(111), while for layers exceeding a thickness of 2 nm, the precision of the orientation is lost.¹⁶ By contrast, reorientation toward a bulk-like structure occurs immediately beyond the first monolayer of HBC on Ag(111).¹⁸ More promising, a vertical stacking of HBC on HOPG and MoS_2 was reported even for film thicknesses of about 10 nm, evidenced by angular resolved NEXAFS and UPS data,²⁰ which is further corroborated by differential reflectance spectroscopy measurements for the case of HOPG.²¹ In view of the large mass of HBC (522.6 u), thermally activated diffusion is expected to enhance film ordering. However, a pronounced dewetting was found upon postgrowth annealing experiments for HBC on HOPG,²⁰ while neither systematic temperature-dependent growth experiments nor growth dynamics studies or XRD data are yet available.

Therefore, in this study we combined X-ray reflectivity (XRR), grazing incidence X-ray diffraction (GIXD), atomic force microscopy (AFM), and near-edge X-ray absorption fine structure (NEXAFS) measurements to analyze the structure and growth evolution of HBC films. In particular we aim to elucidate the effect of surface symmetry and lattice matching on molecular orientation, crystal structure, and morphology by comparing film growth on SiO_2 and HOPG. Both substrates are rather inert thus excluding additional chemical interaction, have similar surface energies of 45.9 mJ m^{-2} for SiO_2 and 54.8 mJ m^{-2} for HOPG, but exhibit quite different surface symmetry properties.^{22,23} On SiO_2 we observe in real-time XRR experiments a transition from lying molecules in the first monolayer to upright standing molecules in the bulk structure, while on exfoliated HOPG substrates HBC forms crystalline multilayers of flat-lying molecules that exhibit a structure similar to the monolayer. With increasing substrate temperature during

film growth the crystallinity but also the film roughness increase. In a previous work it was demonstrated for the case of various acenes that furthermore the surface roughness of HOPG has a severe impact on the molecular orientation and film morphology.²⁴ To scrutinize this correlation for the case of HBC, we have also analyzed films that were grown on defective HOPG(0001), where the coherence of the templating graphite surface lattice was destroyed by ion sputtering, and as a result the HBC molecules revert to arrange uprightly in the bulk structure as observed on SiO_2 .

2. EXPERIMENTAL SECTION

All HBC films were grown under high vacuum conditions (base pressure below 10^{-8} mbar) onto (100)-oriented Si wafers with a native oxide layer and HOPG substrates by molecular beam deposition. For the synthesis of HBC, an alternative synthetic route was pursued, which is described in the Supporting Information. Prior to the film deposition the SiO_2 substrates were rinsed in ultrasonic baths with acetone, isopropanol, and Milli-Q water for at least 15 min. Atomically smooth graphite surfaces were prepared via exfoliation of HOPG substrates (SPI supplies, ZYA quality, mosaic spread $<0.4^\circ$) in air. After loading into the vacuum chamber all substrates were heated at 720 K to remove residual contaminations. To create defective HOPG substrates with reduced templating, some of the cleaved HOPG substrates were intentionally roughened by Ar^+ sputtering ($E = 700 \text{ eV}$, $I = 3 \mu\text{A}$) for 5 min leading to a loss of surface coherence as indicated by the disappearance of the LEED pattern (more information in Supporting Information, Figure S7, and ref 24). After careful outgassing²⁵ HBC was evaporated at a crucible temperature of around 670 K in order to achieve a constant molecular flux of 1 \AA min^{-1} as monitored by a quartz crystal microbalance (QCM), which was increased to about 2 \AA min^{-1} for films with higher thicknesses. The nominal film thickness as determined by the QCM was further cross-calibrated using the XRR measurements on SiO_2 by evaluation of the Kiessig fringes with the Parratt formalism.²⁶

The morphology of the various films was characterized by AFM. All AFM measurements were performed at ambient conditions using either a MultiMode 8 System (Bruker) or an SPM 5500 System (Agilent) operated in tapping mode. Olympus-etched silicon cantilevers with a spring constant of 2 N m^{-1} with typical resonance frequencies of 70 or 300 kHz, respectively, 26.1 N m^{-1} and 260 kHz, as well as MikroMasch cantilevers with resonance frequencies of about 325 kHz and spring constants of 40 N m^{-1} were used. For height calibration of the AFM piezo monatomic steps on HOPG and Au(111) with corresponding interlayer spacings of 3.4 and 2.4 \AA were used. x - y piezo calibration up to an accuracy of 5% was performed using a platinum-coated silicon calibration reference (Digital Instruments).

Crystalline film structure and growth mode were investigated by means of XRR and GIXD measurements performed in a vacuum chamber using Cu $K\alpha$ radiation ($\lambda = 1.542 \text{ \AA}$) created by a rotating anode and the SLS synchrotron source ($\lambda = 0.775 \text{ \AA}$) in Switzerland.²⁷ Additional measurements were performed with a Bruker D8 Discovery diffractometer using Cu $K\alpha$ radiation. In XRR the true specular reflectivity was extracted by subtracting the separately measured diffuse scattering intensity. A footprint correction was performed to account for the illumination geometry at low incident angles. To complement the static, postgrowth picture provided by these methods, we also recorded the specular in situ real-time X-ray growth

oscillations.²⁸ These periodic oscillations of the X-ray reflectivity arise as consecutive molecular MLs are formed on the substrate, thus enabling us to follow the layer coverage and film roughness evolution during deposition.

The NEXAFS measurements were performed at the HE-SGM dipole beamline of the synchrotron storage ring BESSY II in Berlin (Germany) providing linear polarized light (polarization factor = 0.91 and an energy resolution at the carbon K-edge of about 300 meV). All NEXAFS spectra were recorded in partial electron yield mode using a channel-plate detector with a retarding field of -150 V. For the calibration of the absolute energy scale, the photocurrent from a carbon-coated gold grid in the incident beam (absorption maximum = 284.9 eV) was recorded simultaneously. To determine the average molecular orientation relative to the sample surface, NEXAFS spectra were recorded at different angles of incidence (30° , 55° , 70° , and 90°), and the observed dichroism was analyzed after flux normalization and considering the transmission of the monochromator.²⁹ Contributions from the substrate which overlap with the sample signature were subtracted to isolate the sample spectra (more details in the Supporting Information and ref 29).

3. RESULTS

3.1. Film Morphology. First we characterize the morphology of the HBC films by means of AFM. Figure 2 depicts a comparison of atomic force micrographs obtained for various HBC films grown on SiO_2 substrates and HOPG substrates. Deposition of 15 nm of HBC on SiO_2 at $T_s = 300$ K (substrate temperature during film growth) yields a film that consists of uniformly distributed grains with typical lateral diameters of 15–30 nm and heights of about 10 nm (Figure 2a). In addition, about 2% of the surface area is covered with significantly larger crystallites exhibiting diameters of up to 100 nm and heights greater than 20 nm. For a growth temperature of $T_s = 353$ K (Figure 2b) the size of the formed HBC islands increases to typical length scales of about 100 nm. This trend continues upon further increasing the growth temperature to $T_s = 423$ K (Figure 2c), where non-contiguous elongated islands extending over about 500 nm are formed, which indicates ripening of HBC crystallites on the SiO_2 surface. On the surface of the extended islands, steps with a height of 12–14 Å were found, which concurs with the interlayer spacing of (001)_{HBC} planes and thus indicates upright standing molecules in the films. This trend observed from morphology measurements indicates that at elevated substrate temperatures during deposition the crystallinity of the HBC film is enhanced.

Figures 2d and e show the morphology of HBC films grown on pristine, i.e., freshly exfoliated HOPG, with nominal thicknesses of 10 and 75 Å, respectively. In contrast to HBC layers on SiO_2 , large HBC islands are formed on HOPG extending over more than a micron (for comparison, an AFM micrograph of bare HOPG is presented in the Supporting Information, Figure S5). The mesa-like HBC islands are limited in their lateral extensions at the HOPG grain boundaries (cf. Figure 2d and Supporting Information, Figure S6). Therefore, we can safely exclude that the observed step heights result from buried steps of the HOPG surface and know that they indeed represent molecular steps of the HBC film. Several line scans across HBC island edges reveal distinct steps between consecutive HBC layers on the surface of these islands with a height of about 3.5 Å (see line scans V, VI, and VII in Figure 2d, height histogram in Supporting Information, Figure S6).

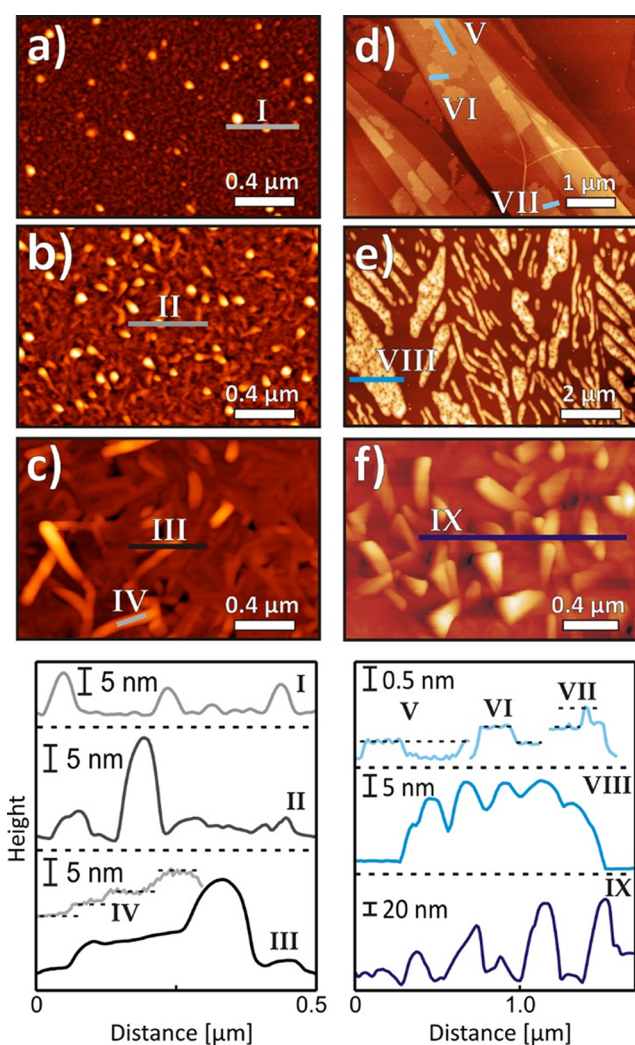


Figure 2. Comparison of AFM micrographs showing the morphology of 15 nm thick HBC films grown at different temperatures on SiO_2 : (a) 300 K, (b) 353 K, and (c) 423 K. Surface morphology of a (d) monolayer (1 nm) and (e) multilayer (7.5 nm) HBC film on pristine HOPG and on sputtered HOPG (80 nm) (f), grown at 300, 300, and 423 K. Corresponding height profiles are shown in the bottom panels. Note that the higher roughness of the sample in (f) results from the higher thickness of that sample.

We note that these values are very close to the interlayer spacing of the basal plane of graphite (3.35 \AA)¹⁹ and the distances observed in columnar HBC aggregates on metal surfaces.^{11,15,30} This indicates that the exclusive recumbent molecular orientation adopted in the first ML of HBC on graphite^{19,20} is pursued throughout the first few monolayers.

The thicker HBC film (75 Å) grown on pristine HOPG consists of separated but rather smooth islands (Figure 2e). About 40% of the surface is covered with elongated islands exhibiting lateral extensions up to several microns. The analysis of the azimuthal distribution of the long island axes exhibits a discrete angular orientation, which mirrors the symmetry of the HOPG surface and thus suggests lattice matching between the substrate surface and film structure. While the sample presented in Figure 2e has been prepared at $T_s = 300$ K, equivalent samples have also been prepared at elevated temperatures. In this case, higher temperatures have resulted in enhanced crystallite size and stronger dewetting (data presented in Supporting Information, Figure S5). In addition, on all islands

characteristic circular pits with several 10 nm in diameter are observed, whose depth could not be resolved due to the finite AFM tip shape and size. Keil et al.²⁰ also observed these depressions as well as a morphological reordering upon subsequent annealing at 425 K, resulting in needle-like aggregates perfectly oriented along the 3-fold symmetry of the HOPG.

To elucidate the influence of the substrate coherence on film growth, complementary films have been prepared on intentionally roughened HOPG surfaces.²⁴ Figure 2f shows a micrograph of 80 nm HBC deposited at $T_s = 423$ K onto a sputtered HOPG surface. A comparison with a HBC multilayer film prepared on SiO₂ (cf. Figure 2c) shows that the morphology of these samples is very similar. Note that this agreement is also found for HBC films deposited at lower substrate temperatures, which feature a morphology similar to the corresponding films prepared on SiO₂ presented in Figure 2a (cf. Supporting Information, Figure S5). This result highlights the importance of substrate microroughness on the resulting templating effect.

3.2. Crystalline Structure. To obtain additional information on the crystalline order within the islands we employed XRR and GIXD measurements below the total reflection edge.³¹ The respective scattering geometries are schematically shown in Figure 3c and d. The out-of-plane XRR measurements of HBC on SiO₂ (Figure 3a, top panel) reveal a (001)_{HBC} Bragg reflection at all temperatures, indicating the formation of crystalline islands composed of upright standing molecules. When increasing the sample temperature during growth, also higher-order diffraction peaks become visible, reflecting the improved crystalline ordering.

The inspection of the in-plane structure (that is, lattice planes aligned perpendicular to the surface) furthermore allows us to identify the exact polymorph. In these GIXD measurements on SiO₂ presented in Figure 3b, the (41-1)_{HBC}, (31-1)_{HBC} and (51-1)_{HBC} diffraction peaks are observed at the positions of the known HBC bulk structure,³² showing that such HBC films adopt the bulk crystal structure. While the first reflection is present in all measurements independent of substrate temperature, the latter can be identified only for $T_s = 423$ K, due to the higher crystallinity of this film as visible in AFM data.

On pristine HOPG, we observe a single strong Bragg reflection corresponding to the (0002)_C spacing (see Figure 3a, bottom panel). Apart from an additional weak reflection due to $\lambda/2$ content in the X-ray beam at $q_z = 0.93 \text{ \AA}^{-1}$ (denoted by the black arrow), no further Bragg reflections are found in XRR. This might be explained by HBC molecules in either disordered configurations or in perfectly flat orientation with essentially the same vertical layer spacing as the HOPG substrate, suggesting a new surface-induced polymorph without herringbone arrangement. As distinct islands are observed in the AFM measurements, a complete absence of crystalline order can be excluded. Further evidence for this thought provide in-plane GIXD measurements, which show an additional diffraction peak at $q_{x,y} = 0.53 \text{ \AA}^{-1}$ (see Figure 3b, bottom panel). This new Bragg peak corresponds to a lateral interlayer spacing of $d = 11.8 \text{ \AA}$, which is close to the HBC diameter and therefore indicates molecules in a lying orientation. We note that this value is very close to the lattice spacing of the (001)_{HBC} bulk lattice plane. However, since we know from GIXD that crystalline ordering exists, the absence of bulk polymorph reflections in the reflectivity scan along q_z indicates that a

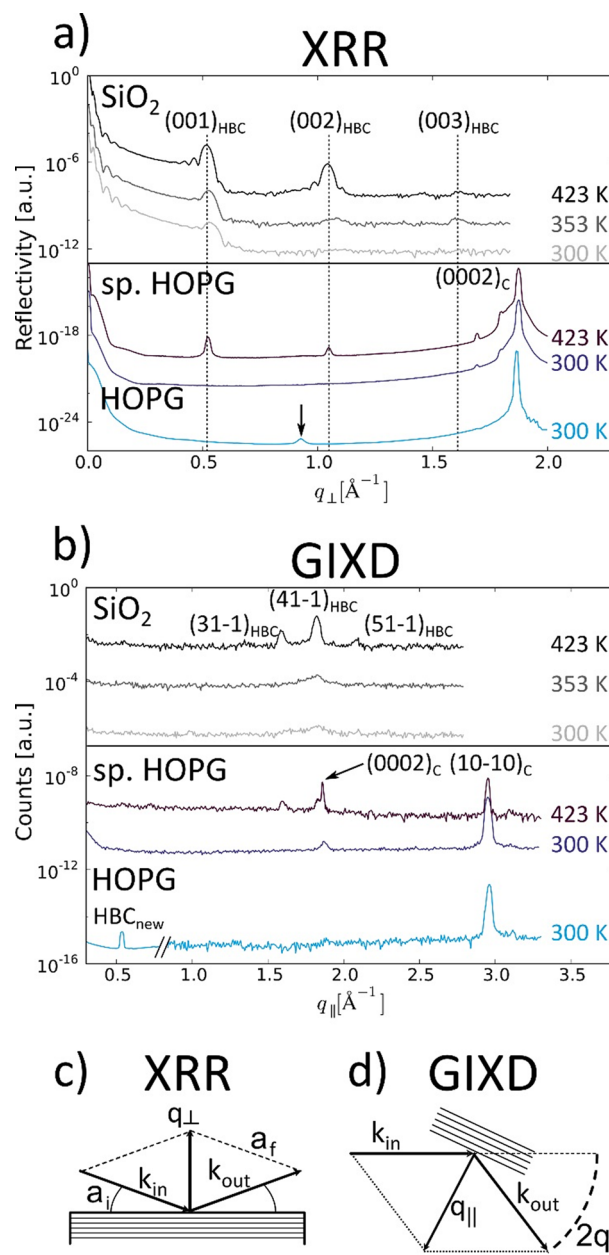


Figure 3. (a) XRR and (b) GIXD measurements of HBC films grown on SiO₂ (top panels, samples correspond to AFM micrographs in Figure 2a–c) at varying temperatures of 300, 353, and 423 K and pristine/defective HOPG (bottom panel samples correspond to AFM micrographs in Figure 2d–f) at 300 K and defective HOPG at 423 K. The scans are offset from each other for clarity. Schematic of the out-of-plane scattering geometry (c) for the XRR measurements and in-plane (d) for the GIXD measurements.

polymorph different from the bulk crystalline structure is present, which is further evidenced by NEXAFS spectroscopy (see below). Therefore, we can explicitly exclude that this peak corresponds to the (001)_{HBC} bulk reflection. Consequently, we cannot use that indexation but denote it as HBC_{new}.

By contrast, in XRR measurements on defective HOPG, again the (00*n*)_{HBC} reflections are found. Additionally, the (31-1)_{HBC} and (41-1)_{HBC} peaks are identified in GIXD scans, proving that HBC grows in upright orientation and adopts the bulk polymorph on defective HOPG, exactly like on SiO₂. This shows that destroying the coherence of the HOPG substrate

lattice by sputtering inhibits nucleation of the molecules in lying configurations. Instead, they adopt an upright configuration in the known bulk structure.

3.3. Molecular Orientation. Though morphological investigations and analysis of X-ray diffraction patterns give an indication for the formation of a new polymorph with coplanar molecular arrangement on pristine HOPG surfaces, these reflections do not provide direct proof for this hypothesis. To allow an independent confirmation of this circumstance, X-ray absorption measurements at the carbon edge (C 1s-NEXAFS) have been performed. In this technique, carbon core electrons are excited into unoccupied molecular orbitals. As the intensity of these excitations depends on the relative orientation between the polarization of the incident X-ray beam and the molecular transition dipole moment (TDM), the molecular orientation can be determined if the resonance intensities recorded at different relative angles are evaluated.^{33,34} Compared to XRD, NEXAFS provides the specific advantage that the structural determination is not restricted to crystalline regions but also probes amorphous regions. Thus, the determined orientation is an average over all molecules exposed to the X-ray beam. Therefore, molecular orientations determined by NEXAFS are often slightly different from those obtained by XRD. As a consequence, substrate defects resulting in different molecular orientation may lead to deviant results.^{24,29}

From previous NEXAFS studies on HBC,³⁵ it is known that the resonances occurring around 284–286 eV correspond to excitations of C 1s electrons into unoccupied π^* orbitals, of which TDM is oriented perpendicular to the molecular plane (see inset in Figure 4a). For multilayers deposited on SiO₂, NEXAFS spectra taken at normal incidence ($\Theta = 90^\circ$) reveal strong π^* resonances, while at lower incident angles of $\Theta = 30^\circ$ these resonances diminish greatly, as shown in Figure 4a. This kind of dichroism is characteristic for upright standing molecules. A quantitative analysis of the dichroism (further details in the Supporting Information) yields an average molecular tilt of $\alpha = 73^\circ \pm 7^\circ$ toward the substrate plane. Therefore, the observed dichroism shows that additionally to molecules in upright orientation (85° in the case of HBC(001)) some molecules exist in recumbent orientations, probably in an amorphous configuration. For a 10 nm thick HBC film deposited onto pristine HOPG an inverted dichroism compared to the SiO₂ samples is found as shown in Figure 4b, revealing an average molecular tilt of $\alpha = 16^\circ \pm 4^\circ$ ^{7,36} toward the substrate basal plane. Remarkably, this recumbent orientation is found to remain stable even in thicker films up to 50 nm in thickness. We would like to point out that this determined molecular orientation cannot be explained by any molecular arrangement in the HBC bulk structure and therefore unambiguously proves that HBC crystallizes in a new polymorph on HOPG surfaces, where the molecules adopt a nearly planar orientation relative to the substrate and each other (this will be discussed in more detail in the Discussion). To improve the statistical reliability of the determined angle, in this case additionally a quasi-continuous measurement combining 26 individual spectra of the dichroism has been performed (data presented in Figure S10, Supporting Information), which perfectly supports the prior finding.

The apparent deviation of the determined average angle from perfectly flat oriented molecules can be explained by the existence of defects on the HOPG surface, where the coherence between substrate and adsorbate is reduced and therefore

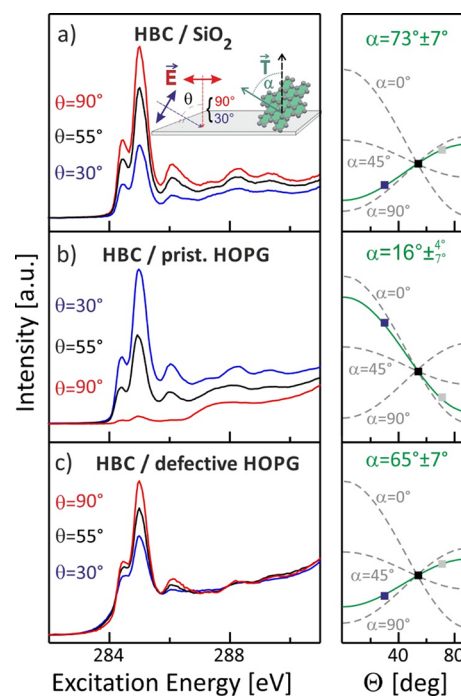


Figure 4. Summary of C 1s NEXAFS spectra of 10 nm thick HBC films grown on (a) SiO₂ and (b) pristine HOPG at varying incident angles between 30° and 90°. Note the inverse dependency of the absorption on the incident angle compared to (a). (c) HBC on defective HOPG shows a dichroism more similar to films on SiO₂ than on pristine HOPG. For clarity the absorption spectra at $\theta = 70^\circ$ (gray squares in the right panels) are not shown. The inset in (a) sketches the experimental geometry and the TDM orientation.

orientations $>0^\circ$ are found. To verify this hypothesis, further NEXAFS measurements have been performed on defect dominated HOPG created by ion sputtering.²⁴ In fact, a drastically different molecular orientation of $\alpha = 65^\circ \pm 7^\circ$ is observed, which corresponds to mostly upright oriented molecules as in the case of SiO₂ substrates, again showing the comparability of HBC films deposited on SiO₂ and defective HOPG.

At higher energies, resonances corresponding to excitations into Rydberg states and σ^* orbitals (>290 eV) occur (data presented in Figure S11, Supporting Information). The TDMs of these excitations lie parallel to the molecular plane but do not exhibit a unique direction. Therefore, in an upright molecular orientation, no strong dichroism of these resonances is found. In recumbent geometries however—like in the case of HBC/HOPG—a clear dichroism, which is inverse compared to the one of the π^* resonances, is observed.

3.4. Evolution of Surface Morphology. To obtain complementary information about the film growth dynamics the X-ray reflectivity at fixed q -points was recorded during HBC deposition. These experiments provide details about the evolution of the surface morphology, which is often difficult to access in postgrowth experiments because thin organic layers can undergo considerable postdeposition reorganization, such as dewetting.^{37–39} The results are shown in Figure 5. We observe X-ray growth oscillations indicating local layer-by-layer (LBL) growth, which is a desirable growth mode because it permits the fabrication of low roughness highly ordered structures, essential for, e.g., multilayer stacks in applications.

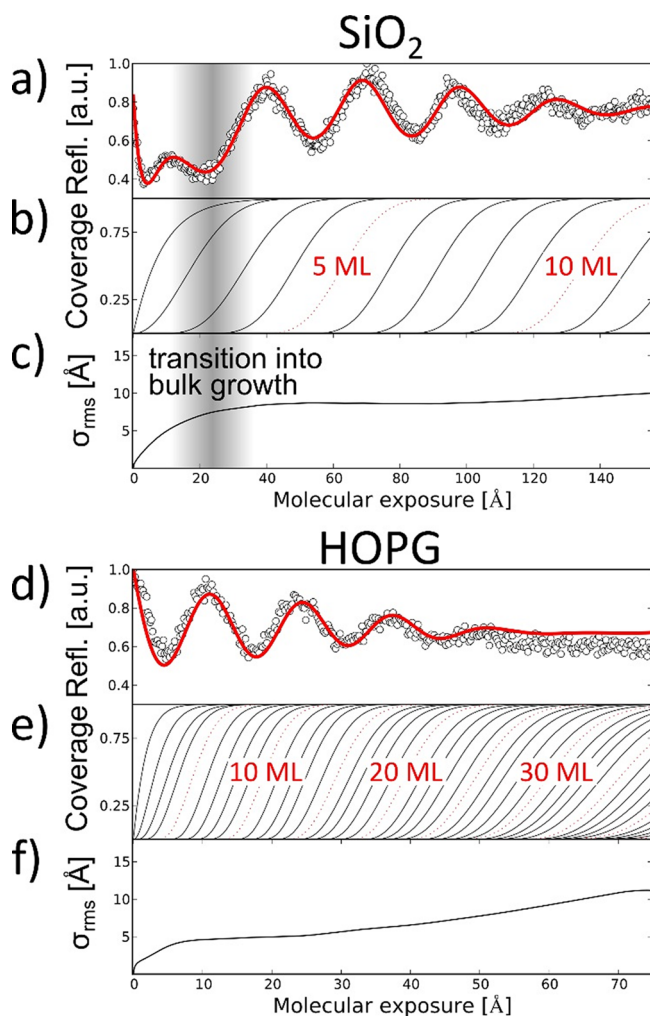


Figure 5. Top: anti-Bragg ($q_z = 0.265 \text{ \AA}^{-1}$) growth oscillations of 150 Å HBC on SiO₂ grown at 300 K. Bottom: Growth oscillations ($q_z = 0.285 \text{ \AA}^{-1}$) of 75 Å HBC grown on pristine HOPG at 300 K. (a), (d) Oscillations and fit of the Trofimov model (for details see the Supporting Information). (b), (e) Calculated layer coverages. (c), (f) Calculated rms roughness.

The anti-Bragg growth oscillations on SiO₂ shown in Figure 5a clearly indicate LBL growth with a decrease in oscillation amplitude for larger film thickness due to increasing roughness. Moreover, a distinctly smaller amplitude of the first oscillation is noticeable, which points toward a different growth behavior of the first ML, compared to thicker films. This transition into the bulk structure when growing HBC on fused quartz has also been observed by Forker et al. using optical spectroscopy.²¹ To obtain satisfactory modeling of the experimentally observed oscillations shown in Figure 5a, an interfacial HBC layer with different orientations from the successive MLs had to be assumed. The best fit⁴⁰ was obtained with d -spacings of $d_1 = 3.4 \text{ \AA}$ and $d_{-1} = 12.5 \text{ \AA}$, which agree with the $d_{(001)}$ -spacing of 11.93 Å obtained by the XRR and GIXD measurements. These values indicate that the molecules are lying down in the first ML, which is also supported by a higher effective growth rate of the first ML (the full fit parameter table is provided in the Supporting Information). A nearly vanishing critical coverage of $\theta_{c,1}$ means that the second upright standing HBC layer starts to grow quasi simultaneously with the lying-down interfacial layer, which therefore acts as a seed layer to initiate the crystal bulk

growth. The region where this transition occurs is highlighted in gray in Figure 5. From the model the surface roughness during film growth can be calculated as shown in Figure 5c.^{41,42} It can be seen that after the transition from lying to upright standing molecules the roughness remains virtually constant after 10 completely filled MLs. Along with the low critical coverages, this means that standing upright molecules grow in a rather smooth quasi layer-by-layer fashion.

Figure 5d shows the growth oscillations during the deposition of 75 Å HBC on pristine HOPG at 300 K, where the best fit was achieved with a vertical layer spacing of $d = 3.37 \text{ \AA}$, corresponding to flat-lying molecules as determined from XRD and NEXAFS. This finding perfectly supports our identification of a new polymorph with coplanar-stacked HBC molecules. The critical coverages are below 1% for all layers, indicating that succeeding layers nucleate well before the lower layer is filled, which is characteristic for a more pronounced 3D island growth. However, since we observe distinct growth oscillations, a classification as quasi LBL is justified.

At elevated temperatures of 353 and 423 K on SiO₂ and at 353 K on HOPG the growth oscillations are damped considerably stronger (see Supporting Information, Figure S12). This can be explained by a more pronounced 3D island growth, which results in a faster increase in surface roughness, as found in the AFM data (see Figure 2).

4. DISCUSSION

Our comprehensive analysis of HBC thin films revealed significant differences in the morphology and crystalline ordering on SiO₂ and HOPG substrates. The molecular step heights observed in AFM micrographs indicate an upright molecular orientation of HBC molecules on SiO₂ and a lying-down orientation on HOPG substrates. This interpretation is further corroborated by XRD and NEXAFS measurements. The observation of $(00n)_{\text{HBC}}$ reflections in XRR data and the appearance of distinct in-plane diffraction peaks reveal that HBC films on SiO₂ crystallize in the bulk phase with a (001) texture. In such planes the molecules are uprightly oriented, which is in good congruence with the average molecular orientation of $\alpha = 73^\circ \pm 7^\circ$ determined independently by NEXAFS spectroscopy, and form a herringbone arrangement as depicted in Figure 6a. Such a film structure is commonly found for π -conjugated molecules, when they are deposited onto inert substrates, where the molecule–substrate interaction is weaker than the mutual molecule interaction^{28,42,43} and can be

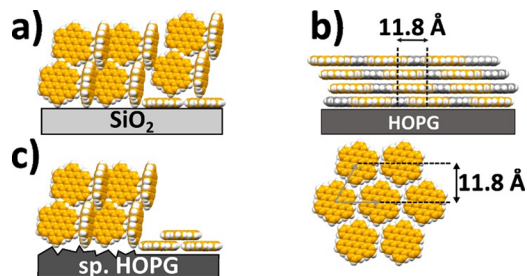


Figure 6. Proposed molecular arrangements of HBC on (a) SiO₂, (b) (top) pristine HOPG, and (c) defective HOPG. (b) (bottom) Sketch of the lateral arrangement of HBC on HOPG. Gray arrows denote the unit cell of a monolayer,¹⁹ and the dashed line represents the distance corresponding to the observed in-plane peak at $q_{xy} = 0.53 \text{ \AA}^{-1}$.

rationalized by minimization of the surface free energy. On the other hand, for HBC films grown on HOPG no additional diffraction peaks besides the substrate (0002)_C reflections were observed in the XRR measurements. This indicates either the presence of almost amorphous HBC films or results from virtually identical vertical layer spacings in HOPG and HBC films. As the AFM micrographs clearly evidence the formation of smooth and well-ordered islands, the former reason can be safely excluded. This finding therefore suggests a planar stacking of HBC molecules, which consequently implies a new packing motif. The NEXAFS measurements provide an independent proof for this new arrangement. The quantitative analyses of multilayer films on HOPG surfaces have yielded an average orientation of the molecular ring plane with respect to the HOPG surface of $\alpha = 16^\circ \pm 4^\circ/7^\circ$ and therefore correspond to a lying conformation. This determined orientation cannot be explained by any crystallographic plane of the HBC bulk structure. Due to the herringbone motif with nearly perpendicular herringbone angle, which the molecules adopt there, no dichroism corresponding to average tilt angles below 42° is possible, even if one of the molecules was aligned perfectly parallel to the surface or both molecules would adopt a zigzag motif with minimal angle relative to the surface. This is accentuated by the following consideration: The correlation between the relative resonance heights for different measurement angles (dichroism) and the corresponding molecular orientation is strongly nonlinear. Consequently, e.g., a relative change of the resonance heights at 30° and 90° by a factor of 2 does not result in a change of the determined molecular orientation of 2. The relative ratio we observe for HBC/HOPG is 18.5, while the molecular arrangement in the bulk phase with the lowest effective TDM orientation (42°) exhibits a relative ratio of 2.1 (further details with computed NEXAFS spectra for different potential molecular packings in Supporting Information). Therefore, the determined angle of 16° unambiguously proves that the molecules have crystallized in a new polymorph with a coplanar orientation on HOPG. We note that this situation closely resembles the adsorption of perfluorinated pentacene on HOPG substrates, where also a new coplanar polymorph instead of the bulk herringbone polymorph is formed.⁷ The new crystalline phase is further characterized by an additional in-plane diffraction peak at $q_{x,y} = 0.53 \text{ \AA}^{-1}$, which corresponds to a lateral interlayer spacing of $d = 11.8 \text{ \AA}$. Previous studies have shown that HBC monolayer films adopt a lattice-matched structure on HOPG surfaces.^{19,44} The hexagonal ad-layer has a 2D lattice parameter of 13.7 \AA and forms molecular rows with a separation of 11.8 \AA as schematically depicted in Figure 6b. Note that in contrast to low-energy electron diffraction (LEED), where the 2D lattice parameters are observed, the in-plane GIXD measurements of multilayer films detect crystalline planes that are oriented perpendicular to the substrate surface. Therefore, the observed lattice planes with a spacing of $d = 11.8 \text{ \AA}$ clearly show that a substrate-induced coplanar stacking is also maintained in HBC multilayer films. Although the exact stacking motif could not be derived from the present measurements, we suggest a lateral shift and rotation between vertically stacked molecules like in graphite in order to minimize electrostatic repulsion between adjacent molecules, as also predicted for stacked coronene molecules.⁴⁵

Coplanar stacking of HBC has also been observed for thin multilayer films grown on Au(111) and Cu(111).¹⁶ However, on those substrates, this new packing motif is only maintained

in a few layers, whereas a molecular reorientation occurs on Ag(111) immediately beyond the first monolayer.¹⁸ Generally, on metal surfaces molecules are chemisorbed and form a densely-packed seed layer with planar adsorption geometry. As a consequence, the large adsorption energy on metal substrates hampers any relaxation such as lateral displacement or slight lifting of molecules at the interface in order to compensate a possible lattice mismatch between the substrate-induced monolayer structure and energetically favorable molecular film structures. Consequently, further molecules cannot pursue this template structure and will in many cases undergo a transition to upright growth or exhibit a pronounced islanding.⁴⁶ Quite differently, rather smooth HBC multilayer films are formed on HOPG, which is attributed to the close match between the graphite lattice and the carbon frame of HBC, as well as the flexibility to precisely match the molecular lattice,²⁹ enabled by the weak adsorption energy of aromatic molecules on graphite⁴⁷ and the absence of strong chemical reactions between adsorbate and surface as expected in the case of metal substrates. Our analysis shows furthermore that the template effect and the formation of a substrate-mediated polymorph depend, however, critically on the coherence of the substrate lattice, since on defective HOPG substrates HBC grows in an upright orientation with an average tilt of $\alpha = 65^\circ \pm 7^\circ$ and adopts the crystalline bulk phase as on SiO₂.

Analysis of X-ray reflectivity at the anti-Bragg point allowed studying the growth dynamics in situ during the nucleation process. From this scenario we conclude that also on SiO₂ the HBC molecules initially adopt a lying orientation in the first layer which, however, changes into an upright orientation upon further deposition. By contrast, the lying orientation remains stable on HOPG with an interlayer spacing of $d = 3.37 \text{ \AA}$. This independently verifies the identification of a new polymorph of flat-lying HBC molecules and shows the stability of a crystalline, lying arrangement well into the multilayer regime. Finally, we note that the resulting film morphology also depends strongly on the substrate temperature during deposition. According to the large molecular mass of HBC, thermally activated diffusion is expected only at elevated temperatures, as the high mass results in a low value of the pre-exponential factor determining the diffusion rates.⁴⁸ In fact, the size of HBC crystallites formed on SiO₂ increases with growth temperature (see Figure 2). By contrast extended crystalline HBC islands are formed on pristine HOPG already at room temperature, indicating a reasonable mobility of planar molecules. Moreover, increasing the temperature upon growth or postdeposition annealing causes substantial dewetting of such HBC films. This can be rationalized by the low surface coordination of the recumbently oriented molecules which yields a high surface free energy, as shown for the case of pentacene.⁴⁹

The observation of such a strong modification of the crystal structure in multilayer films on HOPG compared to the bulk structure (planar arrangement vs herringbone arrangement) has to our knowledge only been reported for PFP.⁷ While for numerous other compounds like pentacene²⁹ and pentacene-tetrone²⁴ in mono- and multilayers recumbent orientations have been observed on HOPG, these always correspond to the known bulk structures. A planar stacking arrangement in the crystalline lattice is frequently found for substituted PAHs (e.g., PTCDA, pentacene-tetrone) which exhibit notable polarity within the molecular π -system and thus lead to additional electrostatic interactions.⁵⁰ In contrast, at present there is no

comprehensive theory which explains decisively why some compounds nucleate in a new polymorph with planar configuration, which remains stable even in multilayer films while others relax into their bulk structure. It may be expected that in the near future crystal prediction theory will allow for such projections.⁵¹ The present study appears especially important, as quantum calculations of Grimme have shown that in large molecules consisting of more than about 15 atoms the enhanced dispersion between planar stacked molecules exceeds their electrostatic repulsion significantly, which favors stacking of π -conjugated molecules.⁵² This further stresses the requirement for experimental data on well-defined model systems consisting of comparably large organic molecules like HBC. Since our results support this projection, it is expected that our findings will stimulate further theoretical work along this direction. In addition, we provide some correlations between the stability of coplanar packing and the corresponding compounds. One striking similarity between PFP and HBC is the nearly perfect perpendicular herringbone angle between both molecules in the unit cell and their similar slip-stacked pattern (cf. Supporting Information, Figure S13). In other compounds like pentacene, where no interface-mediated polymorph with coplanar stacking is found, such a perpendicular herringbone angle is not present. In the case of PFP it has been argued that the packing motif in the new polymorph is partially inherited from the bulk structure, which rationalizes the stability of the polymorphism (see Supporting Information, Figure S13). Therefore, this may also be expected for the HBC polymorph. Furthermore, the face-on-edge herringbone orientation of HBC in the bulk structure is probably only slightly advantageous to a planar configuration regarding its energetic stability. This is due to the weak polarizability of the C–H bonds as well as the reduced effective contact area between two HBC molecules in a face-to-edge configuration resulting from the discotic shape of HBC, which leads to a comparably weak energetic stabilization of this configuration compared to, e.g., pentacene. This interpretation is further supported by the frequent occurrence of liquid-crystalline phases for discotic molecules similar to HBC. Though these are not perfectly crystalline, they still exhibit distinct molecular arrangements. In the arrangements of such discotic liquid crystals, again coplanar motifs are frequently found.¹² The initial HBC molecules form a flat-lying monolayer, which due to the lattice matching of the molecular carbon frame and the HOPG substrate also results in a laterally well-defined seed layer. This slight constraint compared to free nucleation (as, e.g., in crystal growth) results in nucleation in the energetically nearly equivalent coplanar polymorph.

5. CONCLUSIONS

The present study shows that highly ordered graphite substrates serve as an ideal template for the preparation of well-ordered polycyclic aromatic hydrocarbon films. The combination of weak interaction between the substrate and the adsorbate and the structural compatibility of the substrate surface lattice and the molecular carbon frame enables a nucleation of HBC and other PAHs⁷ in coplanar geometry, even though they exhibit a herringbone arrangement in the bulk structure. In the case of HBC such a coplanar stacking is also maintained in multilayer films, thus yielding a new interface-stabilized polymorph. By contrast, HBC films on SiO₂ form polycrystalline islands, which adopt the known bulk polymorph, hence demonstrating that the choice of the substrate directly

allows controlling the crystalline structure of the HBC films. Although also the lateral placement of the individual molecules affects the coupling of stacked molecules and therefore the charge carrier transport efficiency,^{53,54} such a coplanar stacking is expected to largely enhance this transport property along the surface normal of HBC films on HOPG since the overlap of molecular orbitals is clearly enhanced compared to the herringbone arrangement in the bulk structure.^{7,30,55}

The strategy of obtaining a template-induced coplanar stacked polymorph in organic multilayer films on HOPG substrates appears very promising for supramolecular architecture of new carbon materials and may open new opportunities in material science, e.g., for the preparation of nanographenes in molecular columns. Particularly important for the template effect is, however, a long-range ordering of the graphite substrate since surface defects largely reduce the effect of prealigning of molecules, which instead adsorb in an upright orientation and continue to grow as (001)-oriented films adopting the bulk structure.

■ ASSOCIATED CONTENT

📄 Supporting Information

Details on synthesis, additional AFM data, LEED patterns of pristine and damaged HOPG surfaces, details on NEXAFS measurements, and evaluation and additional data, details, and additional data on in situ X-ray reflectivity measurements. This material is available free of charge via the Internet at <http://pubs.acs.org>.

■ AUTHOR INFORMATION

Corresponding Authors

*E-mail: gregor.witte@physik.uni-marburg.de.

*E-mail: stefan.kowarik@physik.hu-berlin.de.

Author Contributions

^{||}P.B. and T.B. contributed equally. The manuscript was written through contributions of all authors. All authors have given approval to the final version of the manuscript.

Notes

The authors declare no competing financial interest.

■ ACKNOWLEDGMENTS

We acknowledge support by the Deutsche Forschungsgemeinschaft (Grant SFB 951, TP A6, A9 and Z1 & Grant SFB 1083, TP A2), the Helmholtz-Zentrum Berlin (electron storage ring BESSY II) for provision of synchrotron radiation at beamline HE-SGM, and the Swiss Light Source for provision of synchrotron radiation at beamline X04SA.²⁷ We want to thank S. Leake and P. Willmott for experimental support at the Swiss Light Source.

■ REFERENCES

- (1) Dimitrakopoulos, C. D.; Malenfant, P. R. L. Organic Thin Film Transistors for Large Area Electronics. *Adv. Mater.* **2002**, *14*, 99–117.
- (2) Sanchez, C.; Belleville, P.; Popall, M.; Nicole, L. Applications of Advanced Hybrid Organic–Inorganic Nanomaterials: From Laboratory to Market. *Chem. Soc. Rev.* **2011**, *40*, 696–753.
- (3) Ortmann, F.; Bechstedt, F.; Hannewald, K. Charge Transport in Organic Crystals: Theory and Modelling. *Phys. Status Solidi B* **2011**, *248*, 511–525.
- (4) Karl, N. In *Organic Electronic Materials*; Farchioni, F., Grosso, G., Eds.; Springer-Verlag: Berlin, Germany, 2001; pp 283–326.
- (5) Anthony, J. E. The Larger Acenes: Versatile Organic Semiconductors. *Angew. Chem., Int. Ed. Engl.* **2008**, *47*, 452–483.

- (6) Li, H.; Giri, G.; Tok, J. B.-H.; Bao, Z. Toward High-Mobility Organic Field-Effect Transistors: Control of Molecular Packing and Large-Area Fabrication of Single-Crystal-Based Devices. *MRS Bull.* **2013**, *38*, 34–42.
- (7) Salzmann, I.; Moser, A.; Oehzelt, M.; Breuer, T.; Feng, X.; Juang, Z.-Y.; Nabok, D.; Della Valle, R. G.; Duhm, S.; Heimel, G.; Brillante, A.; Venuti, E.; Bilotti, I.; Christodoulou, C.; Frisch, J.; Puschnig, P.; Draxl, C.; Witte, G.; Müllen, K.; Koch, N. Epitaxial Growth of π -Stacked Perfluoropentacene on Graphene-Coated Quartz. *ACS Nano* **2012**, *6*, 10874–10883.
- (8) Müllen, K.; Rabe, J. P. Nanographenes as Active Components of Single-Molecule Electronics and How a Scanning Tunneling Microscope Puts Them To Work. *Acc. Chem. Res.* **2008**, *41*, 511–520.
- (9) Grimsdale, A. C.; Müllen, K. The Chemistry of Organic Nanomaterials. *Angew. Chem., Int. Ed. Engl.* **2005**, *44*, 5592–5629.
- (10) Seyler, H.; Purushothaman, B.; Jones, D. J.; Holmes, A. B.; Wong, W. W. H. Hexa-peri-hexabenzocoronene in Organic Electronics. *Pure Appl. Chem.* **2012**, *84*, 1047–1067.
- (11) The van-der-Waals box dimensions represent 98% electron density. Crystallographic details are: monoclinic unit cell, space group $P2_1/a$, $a = 18.431 \text{ \AA}$, $b = 5.119 \text{ \AA}$, $c = 12.929 \text{ \AA}$, $\alpha = 90^\circ$, $\beta = 112.57^\circ$, $\gamma = 90^\circ$, $V = 1126.4 \text{ \AA}^3$, $Z = 2$, $R = 0.056$: Goddard, R.; Haenel, M. W.; Herndon, W. C.; Krüger, C.; Zander, M. Crystallization of Large Planar Polycyclic Aromatic Hydrocarbons: The Molecular and Crystal Structures of Hexabenzobenzocoronene and Benzo[1,2,3-bc:4,5,6-b'c']dibenzocoronene. *J. Am. Chem. Soc.* **1995**, *117*, 30–41.
- (12) Sergeev, S.; Pisula, W.; Geerts, Y. H. Discotic Liquid Crystals: A New Generation of Organic Semiconductors. *Chem. Soc. Rev.* **2007**, *36*, 1902–1929.
- (13) van de Craats, A. M.; Warman, J. M.; Fechtenkötter, A.; Brand, J. D.; Harbison, M. A.; Müllen, K. Record Charge Carrier Mobility in a Room-Temperature Discotic Liquid-Crystalline Derivative of Hexabenzocoronene. *Adv. Mater.* **1999**, *11*, 1469–1472.
- (14) Shklyarevskiy, I. O.; Jonkheijm, P.; Stutzmann, N.; Wasserberg, D.; Wondergem, H. J.; Christianen, P. C. M.; Schenning, A. P. H. J.; de Leeuw, D. M.; Tomović, Z.; Wu, J.; Müllen, K.; Maan, J. C. High Anisotropy of the Field-Effect Transistor Mobility in Magnetically Aligned Discotic Liquid-Crystalline Semiconductors. *J. Am. Chem. Soc.* **2005**, *127*, 16233–16237.
- (15) Pisula, W.; Menon, A.; Stepputat, M.; Lieberwirth, I.; Kolb, U.; Tracz, A.; Siringhaus, H.; Pakula, T.; Müllen, K. A Zone-Casting Technique for Device Fabrication of Field-Effect Transistors Based on Discotic Hexa-peri-hexabenzocoronene. *Adv. Mater.* **2005**, *17*, 684–689.
- (16) Ruffieux, P.; Gröning, O.; Biemann, M.; Simpson, C.; Müllen, K.; Schlappbach, L.; Gröning, P. Supramolecular Columns of Hexabenzocoronenes on Copper and Gold (111) Surfaces. *Phys. Rev. B* **2002**, *66*, 073409.
- (17) Wagner, C.; Kasemann, D.; Golnik, C.; Forker, R.; Esslinger, M.; Müllen, K.; Fritz, T. Repulsion Between Molecules on a Metal: Monolayers and Submonolayers of Hexa-peri-hexabenzocoronene on Au(111). *Phys. Rev. B* **2010**, *81*, 035423.
- (18) Glowatzki, H.; Gavrilu, G. N.; Seifert, S.; Johnson, R. L.; Räder, J.; Müllen, K.; Zahn, D. R. T.; Rabe, J. P.; Koch, N. Hexa-peri-hexabenzocoronene on Ag(111): Monolayer/Multilayer Transition of Molecular Orientation and Electronic Structure. *J. Phys. Chem. C* **2008**, *112*, 1570–1574.
- (19) Zimmermann, U.; Karl, N. Epitaxial Growth of Coronene and Hexa-peri-benzocoronene on MoS₂(0001) and Graphite (0001): A LEED Study of Molecular Size Effects. *Surf. Sci.* **1992**, *268*, 296–306.
- (20) Keil, M.; Samorí, P.; dos Santos, D. A.; Kugler, T.; Stafström, S.; Brand, J. D.; Müllen, K.; Brédas, J. L.; Rabe, J. P.; Salaneck, W. R. Influence of the Morphology on the Electronic Structure of Hexa-peri-hexabenzocoronene Thin Films. *J. Phys. Chem. B* **2000**, *104*, 3967–3975.
- (21) Forker, R.; Diemel, T.; Fritz, T.; Müllen, K. Optical Evidence for Substrate-induced Growth of Ultrathin Hexa-peri-hexabenzocoronene Films on Highly Oriented Pyrolytic Graphite. *Phys. Rev. B* **2006**, *74*, 165410.
- (22) Kawai, A.; Kawakami, J. Characterization of SiO₂ Surface Treated by HMDS Vapor and O₂ Plasma with AFM Tip. *J. Photopolym. Sci. Technol.* **2003**, *16*, 665–668.
- (23) Wang, S.; Zhang, Y.; Abidi, N.; Cabrales, L. Wettability and Surface Free Energy of Graphene Films. *Langmuir* **2009**, *25*, 11078–11081.
- (24) Breuer, T.; Salzmann, I.; Götzen, J.; Oehzelt, M.; Morherr, A.; Koch, N.; Witte, G. Interrelation between Substrate Roughness and Thin-Film Structure of Functionalized Acenes on Graphite. *Cryst. Growth Des.* **2011**, *11*, 4996–5001.
- (25) Note that initial experiments showed large variations in growth behavior. Initially the HBC was dark yellowish and somewhat grayish. After sublimation (a corresponding mass spectrograph is provided in the Supporting Information) a saturated yellow colored material remained. Since the conducted experiments depend critically on the cleanliness of the material system, the experiments were executed with special care to this requirement.
- (26) Parratt, L. G. Surface Studies of Solids by Total Reflection of X-Rays. *Phys. Rev.* **1954**, *95*, 359–369.
- (27) Willmott, P. R.; Meister, D.; Leake, S. J.; Lange, M.; Bergamaschi, A.; Böge, M.; Calvi, M.; Cancellieri, C.; Casati, N.; Cervellino, A.; Chen, Q.; David, C.; Flechsig, U.; Gozzo, F.; Henrich, B.; Jäggi-Spielmann, S.; Jakob, B.; Kalichava, I.; Karvinen, P.; Krempasky, J.; Lüdeke, A.; Lüscher, R.; Maag, S.; Quitmann, C.; Reinle-Schmitt, M. L.; Schmidt, T.; Schmitt, B.; Streun, A.; Vartiainen, I.; Vitins, M.; Wang, X.; Wullschlegel, R. The Materials Science Beamline Upgrade at the Swiss Light Source. *J. Synchrotron Radiat.* **2013**, *20*, 667–682.
- (28) Kowarik, S.; Gerlach, A.; Sellner, S.; Schreiber, F.; Cavalcanti, L.; Konovalov, O. Real-Time Observation of Structural and Orientational Transitions During Growth of Organic Thin Films. *Phys. Rev. Lett.* **2006**, *96*, 125504.
- (29) Götzen, J.; Käfer, D.; Wöll, C.; Witte, G. Growth and Structure of Pentacene Films on Graphite: Weak Adhesion as a Key for Epitaxial Film Growth. *Phys. Rev. B* **2010**, *81*, 085440.
- (30) Käfer, D.; Bashir, A.; Dou, X.; Witte, G.; Müllen, K.; Wöll, C. Evidence for Band-Like Transport in Graphene-Based Organic Monolayers. *Adv. Mater.* **2010**, *22*, 384–388.
- (31) At an incident angle of $\alpha_i = 0.15^\circ$, well below the total reflection edge at 0.2° , the X-ray penetration depth in HBC amounts to only 67 Å, which ensures that the obtained GIXD signal originates mainly from the HBC ad-layer. However, this is not true for partially covered substrates, such as HOPG, which means that actually a superposition of substrate and molecule diffraction features is observed.
- (32) Desiraju, G. R.; Gavezzotti, A. Crystal Structures of Polynuclear Aromatic Hydrocarbons. Classification, Rationalization and Prediction from Molecular Structure. *Acta Crystallogr., Sect. B: Struct. Sci.* **1989**, *45*, 473–482.
- (33) Stöhr, J.; Outka, D. Determination of Molecular Orientations on Surfaces from the Angular Dependence of Near-Edge X-Ray-Absorption Fine-Structure Spectra. *Phys. Rev. B* **1987**, *36*, 7891.
- (34) Stöhr, J. In *NEXAFS Spectroscopy*; Gomer, R., Ed.; Springer-Verlag: Berlin, Germany, 1992.
- (35) Luo, Y.; Ågren, H.; Keil, M.; Friedlein, R.; Salaneck, W. R. A Theoretical Investigation of the Near-Edge X-Ray Absorption Spectrum of Hexa-peri-hexabenzocoronene. *Chem. Phys. Lett.* **2001**, *337*, 176–180.
- (36) As the dependence of the determined molecular orientation on the individual resonance heights is nonlinear, the errors in the determined values are nonconstant and asymmetric.
- (37) Amassian, A.; Pozdin, V. A.; Desai, T. V.; Hong, S.; Woll, A. R.; Ferguson, J. D.; Brock, J. D.; Malliaras, G. G.; Engstrom, J. R. Post-Deposition Reorganization of Pentacene Films Deposited on Low-Energy Surfaces. *J. Mater. Chem.* **2009**, *19*, 5580–5592.
- (38) Käfer, D.; Wöll, C.; Witte, G. Thermally Activated Dewetting of Organic Thin Films: the Case of Pentacene on SiO₂ and Gold. *Appl. Phys. A: Mater. Sci. Process.* **2009**, *95*, 273–284.

(39) Kowarik, S.; Gerlach, A.; Sellner, S.; Cavalcanti, L.; Schreiber, F. Dewetting of an Organic Semiconductor Thin Film Observed in Real-Time. *Adv. Eng. Mater.* **2009**, *11*, 291–294.

(40) Woll, A. R.; Desai, T. V.; Engstrom, J. R. Quantitative Modeling of In Situ X-Ray Reflectivity During Organic Molecule Thin Film Growth. *Phys. Rev. B* **2011**, *84*, 075479.

(41) Dinelli, F.; Murgia, M.; Levy, P.; Cavallini, M.; Biscarini, F.; de Leeuw, D. Spatially Correlated Charge Transport in Organic Thin Film Transistors. *Phys. Rev. Lett.* **2004**, *92*, 116802.

(42) Kowarik, S.; Gerlach, A.; Hinderhofer, A.; Milita, S.; Borgatti, F.; Zontone, F.; Suzuki, T.; Biscarini, F.; Schreiber, F. Structure, Morphology, and Growth Dynamics of Perfluoro-pentacene Thin Films. *Phys. Status Solidi RRL* **2008**, *2*, 120–122.

(43) Breuer, T.; Witte, G. Thermally Activated Intermixture in Pentacene-Perfluoropentacene Heterostructures. *J. Chem. Phys.* **2013**, *138*, 114901.

(44) Schmitz-Hübsch, T.; Sellam, F.; Staub, R.; Törker, M.; Fritz, T.; Kübel, C.; Müllen, K.; Leo, K. Direct Observation of Organic–Organic Heteroepitaxy: Perylene-tetracarboxylic-dianhydride on Hexa-peribenzocoronene on Highly Ordered Pyrolytic Graphite. *Surf. Sci.* **2000**, *445*, 358–367.

(45) Rapacioli, M.; Calvo, F.; Spiegelman, F.; Joblin, C.; Wales, D. J. Stacked Clusters of Polycyclic Aromatic Hydrocarbon Molecules. *J. Phys. Chem. A* **2005**, *109*, 2487–2497.

(46) Witte, G.; Wöll, C. Growth of Aromatic Molecules on Solid Substrates for Applications in Organic Electronics. *J. Mater. Res.* **2004**, *19*, 1889–1916.

(47) Zacharia, R.; Ulbricht, H.; Hertel, T. Interlayer Cohesive Energy of Graphite from Thermal Desorption of Polyaromatic Hydrocarbons. *Phys. Rev. B* **2004**, *69*, 155406.

(48) Doll, J. D.; Voter, A. F. Recent Developments in the Theory of Surface Diffusion. *Annu. Rev. Phys. Chem.* **1987**, *38*, 413–431.

(49) Ambrosch-Draxl, C.; Nabok, D.; Puschnig, P.; Meisenbichler, C. The Role of Polymorphism in Organic Thin Films: Oligoacenes Investigated from First Principles. *New J. Phys.* **2009**, *11*, 125010.

(50) Käfer, D.; El Helou, M.; Gemel, C.; Witte, G. Packing of Planar Organic Molecules: Interplay of van der Waals and Electrostatic Interaction. *Cryst. Growth. Des.* **2008**, *8*, 3053–3057.

(51) Price, S. L. Predicting Crystal Structures of Organic Compounds. *Chem. Soc. Rev.* **2014**, *43*, 2098–2111.

(52) Grimme, S. Do Special Noncovalent π – π Stacking Interactions Really Exist? *Angew. Chem., Int. Ed.* **2008**, *47*, 3430–3434.

(53) Lemaur, V.; da Silva Filho, D. A.; Coropceanu, V.; Lehmann, M.; Geerts, Y.; Piris, J.; Debije, M. G.; van de Craats, A. M.; Senthilkumar, K.; Siebbeles, L. D. A.; Warman, J. M.; Brédas, J. L.; Cornil, J. Charge Transport Properties in Discotic Liquid Crystals: A Quantum-Chemical Insight into Structure-Property Relationships. *J. Am. Chem. Soc.* **2004**, *126*, 3271–3279.

(54) Olivier, Y.; Muccioli, L.; Lemaur, V.; Geerts, Y. H.; Zannoni, C.; Cornil, J. Theoretical Characterization of the Structural and Hole Transport Dynamics in Liquid-Crystalline Phthalocyanine Stacks. *J. Phys. Chem. B* **2009**, *113*, 14102–14111.

(55) Kirkpatrick, J.; Marcon, V.; Nelson, J.; Kremer, K.; Andrienko, D. Charge Mobility of Discotic Mesophases: A Multiscale Quantum and Classical Study. *Phys. Rev. Lett.* **2007**, *98*, 227402.